Research Article Vol. 30, No. 4 / 14 Feb 2022 / Optics Express 4895
Optics EXPRESS

PCF based modal interferometer for lead ion detection

ABDULLAH AL NOMAN,[1] JITENDRA NARAYAN DASH,[2,3] XIN CHENG,[2,4] HWA-YAW TAM,[2] AND CHANGYUAN YU[1]

[1]*Photonics Research Center, Department of Electronic and Information Engineering, The Hong Kong Polytechnic University, 11 Yuk Choi Rd, Hung Hom, Hong Kong SAR, China*
[2]*Photonics Research Center, Department of Electrical Engineering, The Hong Kong Polytechnic University, 11 Yuk Choi Rd, Hung Hom, Hong Kong SAR, China*
[3]*jnphysics@gmail.com*
[4]*eechengx@polyu.edu.hk*

Abstract: A compact, reliable, and fast responsive PCF (photonic crystal fiber) based modal interferometric sensor for lead ion detection is proposed and experimentally demonstrated. The sensor has been fabricated by splicing a small section of PCF with SMF (single mode fiber) followed by collapsing the air holes of PCF at its tip. The interferometer is dip coated with chitosan-PVA (polyvinyl alcohol) and glutathione functionalized gold nanoparticles. Three probes have been fabricated, and the maximum sensitivity has been found to be 0.031 nm/ppb for lead ions whereas the detection range has been considered from 0 ppb to 50 ppb. The probe has been found to have a faster response time of ~ 10 s. Furthermore, the sensor has been found to be less responsive towards other heavy metal ions, thereby demonstrating its selectivity towards lead ions. Besides, a section of FBG (fiber Bragg grating) has been embedded into the interferometer and the temperature response of FBG peak along with interference spectra has been investigated for better accuracy.

1. Introduction

Over the last decennium, water pollution has emerged as one of the environment's primary threats due to the dramatic increase in the number of industries, mining, agricultural wastes, and fossil fuel combustion. Heavy metals pollution is deemed one of them due to its toxicity and pernicious effect on humans, aquatic life, and nature [1]. The fast accumulation of the heavy metal ions (such as arsenic (As), lead (Pb), cadmium (Cd), and mercury (Hg), etc.) in the ecosystem and non-biodegradability poses a severe threat [2]. Among them, lead (Pb) ion is a well-known and dangerous heavy metal for its significant usage in industrial applications and consequences on human life such as liver, brain, lung, nerves damage, stroke, high pressure, and skin cancer [3,4]. Therefore, international agencies including WHO (World Health Organization) have set the threshold level for lead concentration up to 10 ppb (parts per billion) in drinking and in-situ water [5]. Many diverse and conventional analytical techniques including atomic absorption spectrometry [6], inductively coupled plasma mass spectrometry [7], spectrophotometry [8], fluorescence [9], and electrochemical based methods [10] have been employed for lead ion detection. These approaches are constrained by the complicated fabrication process, expensive detection devices, sizable quantity of substances, and long tracing time for the laboratory and environmental use [11–13]. Thus, it is significant to implement a simple, inexpensive, and susceptible sensor for monitoring lead ions to avoid these drawbacks.

Concurrently, optical fiber based sensors have got the interest over traditional methods for their compactness, minimal expense, immune to electromagnetic interference, and high precision [14–18]. Fiber optic sensors based on various techniques have been demonstrated for lead ion detection. For instance, a TBFG (tilted fiber Bragg grating) coated with BP (black phosphorus)

#447272 https://doi.org/10.1364/OE.447272
Journal © 2022 Received 29 Oct 2021; revised 13 Dec 2021; accepted 30 Dec 2021; published 1 Feb 2022

Optics EXPRESS

nanosheet has been demonstrated for lead concentration tracing [19]. The sensor has achieved a sensitivity of 0.5×10^{-3} dB/ppb with a wide measurement range from 0.1 to 10^7 ppb. Optical fibers based SPR (surface plasmon resonance) sensors have also been reported for lead ion detection using both chitosan and GSH (glutathione) as a coating layer, and the probe has been found to have a sensitivity of 0.28 mV/ppb with the detection range being 1–7 ppb [20]. Also, an ion-imprinted fiber sensor has been reported using similar approach [21]. The above sensors for lead ion detection rely on intensity based interrogation where the results may be vulnerable to fluctuation in intensity of incident light as well as bending of the fiber. Additionally, these devices involve complex fabrication processes and have a longer response time [22].

Meanwhile, optical fiber based interferometric sensors have also been developed for detecting lead ions because of their compact design, quick reaction, and high accuracy [23]. For instance, a microfiber based lead sensor has been demonstrated using functionalized BP layer for lead concentration ranging from 0 ppb to 10 ppb [24]. Moreover, a glutathione coated microfiber based fiber sensor has also been utilized for lead ion detection [25]. Furthermore, an optical fiber based on FPI (Fabry-Pérot Interferometer) has been fabricated for lead ion detection by depositing a thin layer of chitosan on the tip of the fiber, and the sensitivity has been found to be 0.177 dB/ppm (parts per million) with tracing limit confined to 0–1.2 ppm [26]. Nonetheless, all the reported interferometric based sensors have an extensive reaction period, no selectivity, and narrow detection limit.

In this study, a simple and compact reflection based interferometric sensor is proposed to detect heavy metal ion such as lead. The interferometer has been fabricated by splicing a section of SMF with PCF using a commercial splicer machine, while a section of FBG is spliced to this interferometer for temperature monitoring. The PCF is coated by a chitosan-PVA layer followed by a GSH functionalized gold nanosheets. The GSH is an economical biocompatible material that has a selective response towards lead ions through its mercapto group [27]. The sensitivity response of the proposed sensor is recorded based on the shifting in the interference minima. Besides, the selectivity, response time and temperature response have been studied to improve the measurement accuracy of the sensor.

2. Fabrication of materials and chemicals

2.1. Materials

PVA (99%), chitosan (medium molecular weight), gold chloride solution, GSH (l-glutathione, 98%), lead nitrate (99%, for analytical), mercury nitrate monohydrate, cadmium nitrate tetrahydrate, copper nitrate hydrate, acetone, and acetic acid were procured from Sigma Aldrich. All these chemical components were used for the fabrication process without any extra modification. Besides, distilled water is utilized for making the aqueous concentration of heavy metal ions.

2.2. Preparation of coating layers

AuNPs (gold nanoparticles) were synthesized by dissolving chitosan in the gold chloride solution. In this process, 1% wt. of chitosan was added to 4% (v/v) acetic acid solution, and the mixture was stirred for 6 hrs [28]. Subsequently, 40 ml of 1 mM gold chloride was stirred in a beaker at 40°C. Once the solution started evaporating, 4 ml of chitosan was soluted into it. The formation of AuNPs was confirmed when the mixer turned into violet color (see Fig. 1(a)). Subsequently, the solution was cooled at ambient temperature and then was kept in a refrigerator below 4°C for further use [22]. Afterwards, 1 mM GSH was mixed with AuNPs at a 1:1 ratio (v/v) to make functionalized AuNPs (see Fig. 1(b)), and the mixture was stirred overnight at room temperature. The mixture of GSH functionalized AuNPs are stable as the GSH prevent AuNPs from aggregation [27]. On the other hand, GSH functionalized AuNPs has two carboxylic (-COOH) groups, where one group forms bonding with AuNPs surface layer and the other with

Optics EXPRESS

the target lead ion [27]. Moreover, chitosan-PVA solution was prepared by heating and stirring PVA for 4 hrs followed by the addition of chitosan to the hot PVA solution (displayed in Fig. 1(c)).

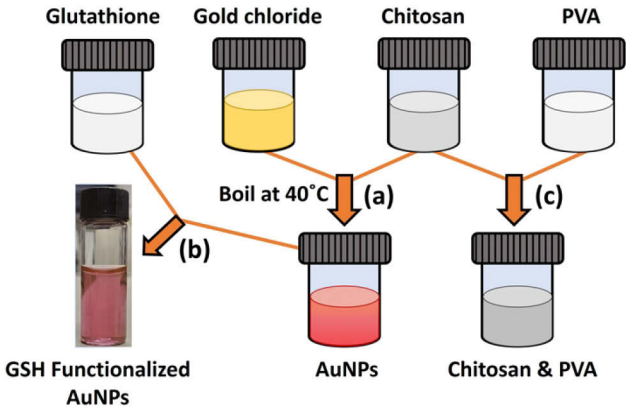

Fig. 1. Steps followed for the synthetization of functionalized AuNPs and chitosan-PVA.

3. Sensing principle, probe fabrication process, and experimental setup

3.1. Principle of the interferometer

The schematic of the proposed SMF-PCF structure along with light propagation is shown in Fig. 2. The core mode of SMF diffracts and broadens at the collapsed region, thereby exciting core and cladding modes in PCF. These modes travel along the PCF and combine again at the collapsed region at the tip of PCF before being reflected back to the PCF. The curved tip of the collapsed area helps in a better collection of reflected light by the PCF. The reflected light is collected at the SMF-PCF junction and a part of this light is filtered into the core of SMF. Due to the difference in the effective index of the core and cladding modes of PCF, these modes accumulate phase difference during their forward and backward propagation leading to the formation of the interference pattern. The evanescent wave of cladding modes is sensitive to the change in the surrounding environment. Therefore, any change in the refractive index of the surrounding medium will lead to the change in the effective index of cladding modes which in turn shifts the resultant interference pattern [29].

3.2. Fabrication of the sensor

The proposed interferometer was fabricated by splicing a section of SMF with a small section of commercial PCF (Newport, model no: F-SM8) using a commercial fusion splicer (FITEL s178A). The average diameter of the core of PCF is 8.6 μm, while the diameter (d) and pitch (Λ) of the holes are 2.39 μm and 5.63 μm, respectively. The cross section of the PCF along with geometrical parameters are shown in Fig. 3(a) and its inset, respectively. The splicing of SMF with PCF leads to the collapse of holes of PCF over a length of 270 μm at the SMF-PCF junction, as shown in Fig. 3(b). Then the PCF was cleaved at a distance of 8 mm from the splicing junction. Afterwards, the tip of PCF was sealed by providing suitable arc discharge, and the length of the collapsed region formed in this process is 153 μm (see Fig. 3(c)). The sealing of the tip of PCF helps to prevent the infiltration of liquid into the holes of PCF. Additionally, a section of FBG (length = 5 mm, pitch = 0.53 μm) was spliced to the SMF before the SMF-PCF junction.

The probe (PCF along with collapsed region) was considered for the dip coating process. Firstly, the probe was first immersed into acetone for 20 mins to remove the contaminants present on its surface. The treated probe was washed with DI water and then dried at 65°C for an hour.

Optics EXPRESS

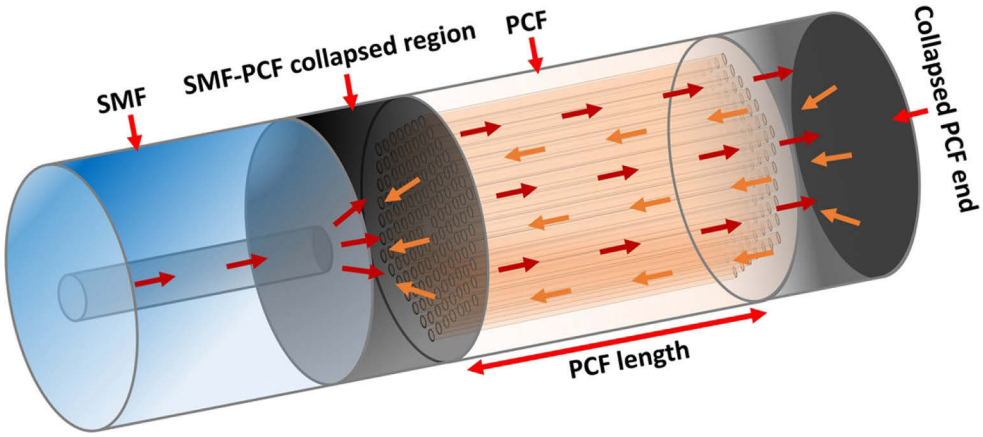

Fig. 2. Schematic of the fabricated SMF-PCF based interferometric sensor.

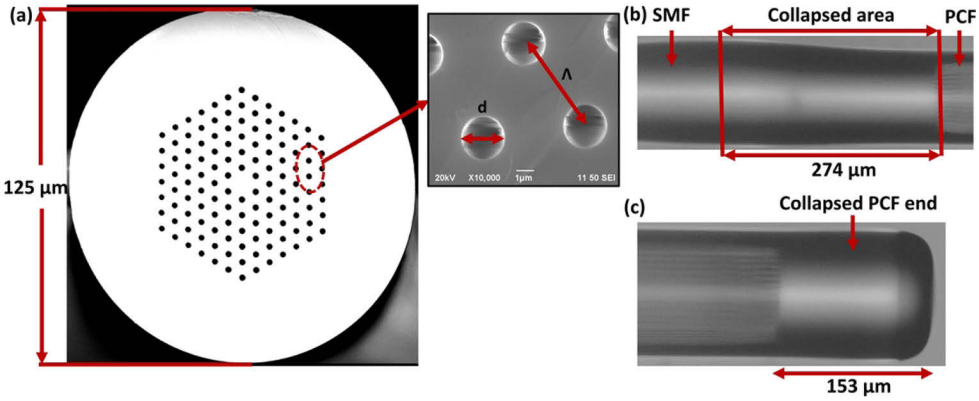

Fig. 3. Cross-sectional view of the PCF (a), collapsed region at the SMF-PCF junction (b) and collapsed region at tip of PCF (c).

Afterwards, the probe was dip coated into the prepared chitosan-PVA mixture for 20 minutes, thereby forming a layer on its surface. The chitosan-PVA layer binds easily to the silica PCF surface due to the good adhesive strength of PVA through its water-soluble synthetic polymer [30]. Then the coated probe was dried in vacuum at 65°C for 30 mins to make the deposition uniform as well as enhance the bonding between the fiber and the coating layer [24]. Thereafter, the dried probe was dipped into the solution of functionalized AuNPs and then dried again in the vacuum chamber. The schematic of the coated layers on PCF is illustrated in Fig. 4(a). Besides, the SEM (scanning electron microscope) images of the coating and the zoomed view of a section of the coating layer are shown in Fig. 4(b). Before the coating the PCF diameter was 125 µm, whereas after the coating the average diameter of the PCF is found to be as 130 µm. Following the above procedure, three probes with similar geometrical parameters are fabricated.

3.3. Experimental setup

The schematic of the experimental setup is shown in Fig. 5(a). The first and third port of a circulator (6015-3-APC, Thorlabs Inc, New Jersey, USA) was connected to a homemade BBS (broadband source, maximum output power ~3 mW) and OSA (optical spectrum analyzer, AQ6370D, YOKOGAWA, Tokyo, Japan), respectively, while the second port was connected

Optics EXPRESS

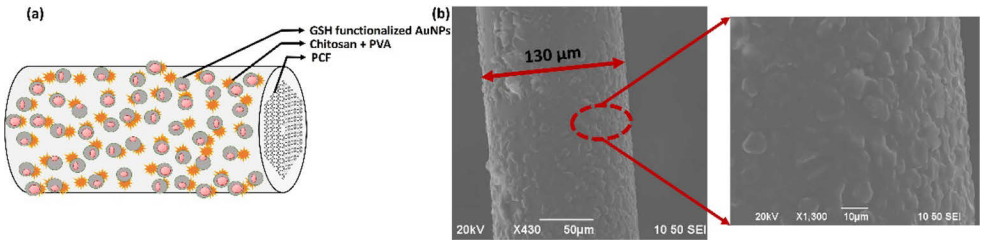

Fig. 4. (a) Schematic of the coated layers on the PCF surface, (b) SEM images of the chitosan-PVA and GSH functionalized AuNPs coated probe.

to the probe. The light launched from BBS gets reflected from the tip of the probe, and the reflected light was collected at the OSA for analysis while keeping the spectral resolution fixed at 0.05 nm. The resultant interference pattern before and after coating materials on the probe is depicted in Fig. 5(b). The sharp peak in Fig. 5(b) corresponds to the FBG incorporated before the interferometer. As can be seen from the figure, there is a change in intensity as well as the shift in interference minima which occurs due to the change in the effective index of cladding mode upon interaction with the surrounding medium.

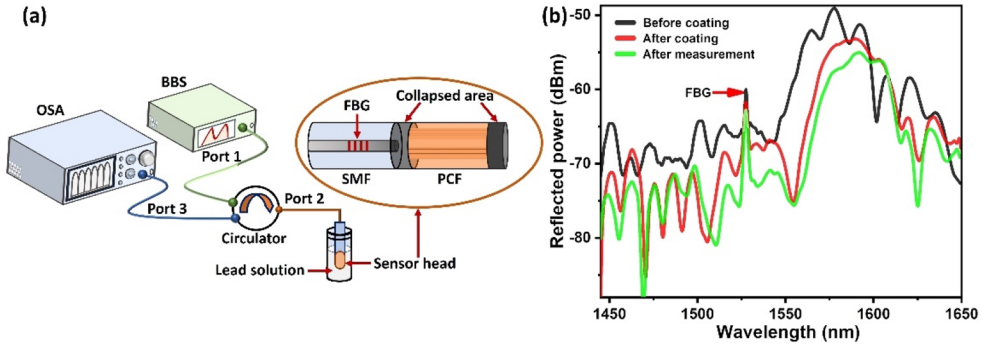

Fig. 5. (a) shows the experimental setup and (b) shows the spectra before and after deposition of the coating layers as well as spectra after measurement.

4. Results and discussion

In order to detect the lead concentration, the fabricated probe was dipped into aqueous solutions with concentrations of lead ranging from 0 ppb to 50 ppb. Upon immersion into various solutions, the interference minima exhibit a red shift with an increase in lead concentration, as shown in Fig. 6(a). The change of the interference minima can be attributed to the interaction between glutathione functionalized AuNPs with lead ions. In particular, two carboxylic (-COOH) groups and one amino group ($-NH_2$) group in the GSH structure facilitates the attachment of lead ions. Thus, when the sensor is submerged in the solutions, the lead (Pb^{2+}) ions forms a bond with chelating ligands of the coated layer thereby changing the effective index of cladding modes of PCF which in turn shifts the interference minima [27]. The above procedure was repeated for three cycles for each probe and the average sensitivity along with the error bar is shown in Fig. 6(b). As can be seen from the figure, the average sensitivity of the three probes are found to be 0.031 nm/ppb, 0.028 nm/ppb, and 0.029 nm/ppb. It may be noted that after each measurement cycle, the interference pattern comes back to its original position (when unexposed to lead solution), thereby confirming the potential for reusability (see Fig. 5(b)). Besides, considering the

Optics EXPRESS

resolution of the OSA ($\Delta\lambda$) and the probe highest sensitivity (s), the LOD (limit of the detection, $\Delta\lambda/s$) for the proposed sensor has been found as 1.6 ppb.

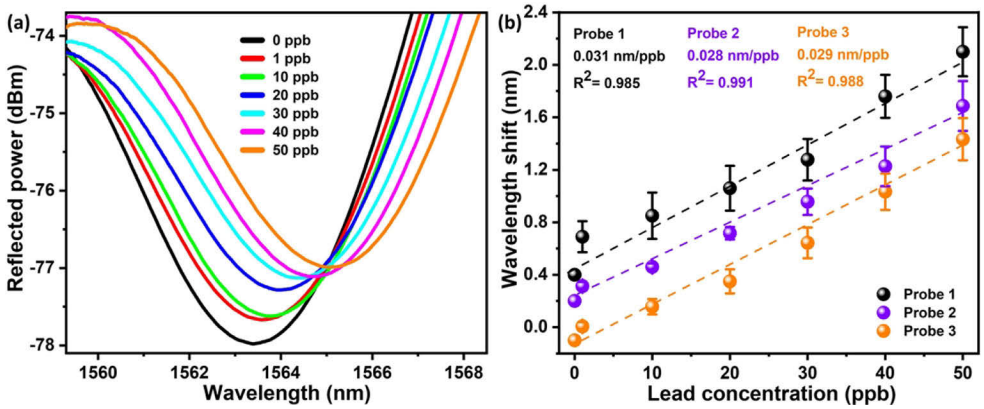

Fig. 6. (a) Shift in the interference spectra for various lead ion concentrations (Probe 1) and (b) shows the average sensitivity of three probes.

In addition to sensitivity, the response time of a probe plays a significant role in practical applications. Therefore, the response time of the proposed probe was investigated by immersing it in solutions with three different concentrations such as 10 bbp, 30 ppb, and 50 ppb and the result is depicted in Fig. 7(a). It can be seen from the figure that the response time of the probe for an increase in the concentration from 10 ppb to 30 ppb and 30 ppb to 50 ppb is found to be 9 s and 12 s (see Fig. 7(b), 7(c)) respectively while it is 9.5 s and 11.5 s for the reversing order (displayed in Fig. 7(d), 7(e)). Therefore, the average response time is around 10 s which is better than the previously reported results [20,22,24–26,31]. The fast response time can be attributed to the quick bond formation between the GSH coated layer and lead ions. Besides, an instability has been noticed in Fig. 7(a) due to sensor transition from air to various lead concentrations and vice versa. Table 1 summarizes the performances of various fiber optic sensors for lead ion detection.

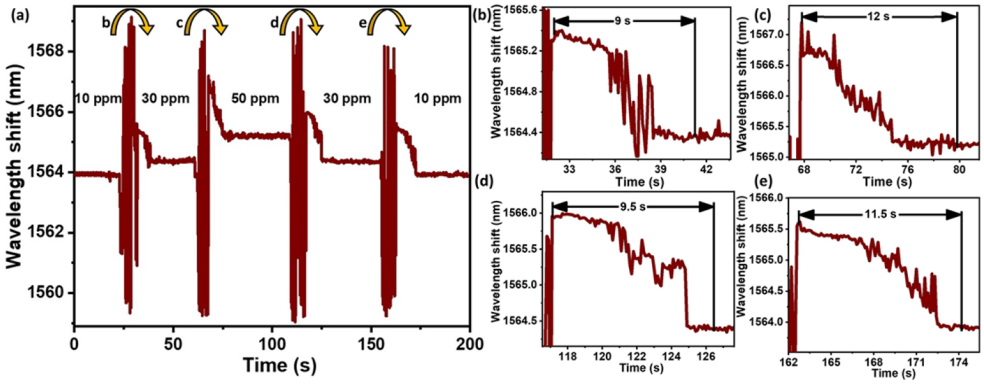

Fig. 7. Response time of the probe for lead concentrations of 10 ppb, 30 ppb, and 50 ppb. (b), (c), (d), and (e) refer to the response time that corresponds to the transition of interference minima for change in concentration from 10 ppb to 30 ppb.

The practicality of the probe for lead ion detection has further been verified by investigating its response towards other heavy metal ions. This was achieved by immersing the probe into aqueous solutions of mercury (Hg^{2+}), copper (Cu^{2+}), cadmium (Cd^{2+}) with concentrations varying from

Optics EXPRESS

Table 1. Performance of the various fiber optic sensors for lead detection.

Method	Sensing structure	Coated material	Concentration range	Sensitivity	Response time	Ref.
Fiber grating based sensors	TFBG	BP	0.1–10^7 ppb	0.5×10^{-3} dB/ppb	-	[19]
	FBG	BP	0 - 5 ppb	-	-	[25]
	LPFG	PMO	0–10^5 ppb	0.01 nm/ppb	-	[32]
SPR based sensor	Multimode POF	Chitosan and GSH	1–7 ppb	0.28 mV/ppb	-	[20]
Interferometer based sensors	Microfiber	BP	0–10 ppb	-	45 s – 56 s	[24]
	FPI	Chitosan	0–1200 ppb	0.17×10^{-3} dBm/ppb	-	[26]
	SMF-PCF	**Chitosan-PVA, GSH functionalized AuNPs**	**0–50 ppb**	**0.031 nm/ppb**	**9 s – 12 s**	**this study**

0 to 50 ppb, and the results are plotted in Fig. 8. It can be noted from the figure that the sensitivity of the proposed probe is nearly three times higher for lead ions than other heavy metal ions due to the strong bonding between lead ions and GSH functionalized AuNPs [27,33], thereby proving its selectivity.

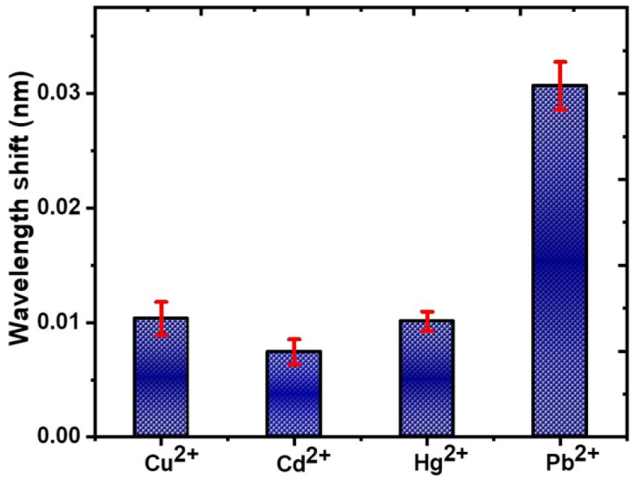

Fig. 8. Response of the sensor towards lead ions and other heavy metal ions.

Afterwards, the response of the sensor towards change in ambient temperature has also been studied by monitoring of the FBG peak and interference spectrum. The interferometer and the FBG were kept in a tube furnace (shown in Fig. 9(a)), and the temperature was increased from 25°C to 45°C at a step of 5°C. Both the interference spectra and the FBG peak shows a red shift with an increase in temperature and have a linear response as shown in Fig. 9(b) and Fig. 9(c) and their insets, respectively. The interference minima corresponding to the coated probe has been found to have an average temperature sensitivity of 11.8 pm/°C (see Fig. 9(b)), while that of FBG peak has been found to be ~ 9.8 pm/°C (see Fig. 9(c)). Considering the response of the sensor to change in lead ion concentrations and change in temperature, the cross-temperature sensitivity has been found to be 0.38 ppb/°C. The presence of FBG helps in evaluating the cross-temperature

Optics EXPRESS

error due to the fluctuation in environmental temperature during the monitoring of lead ion concentration.

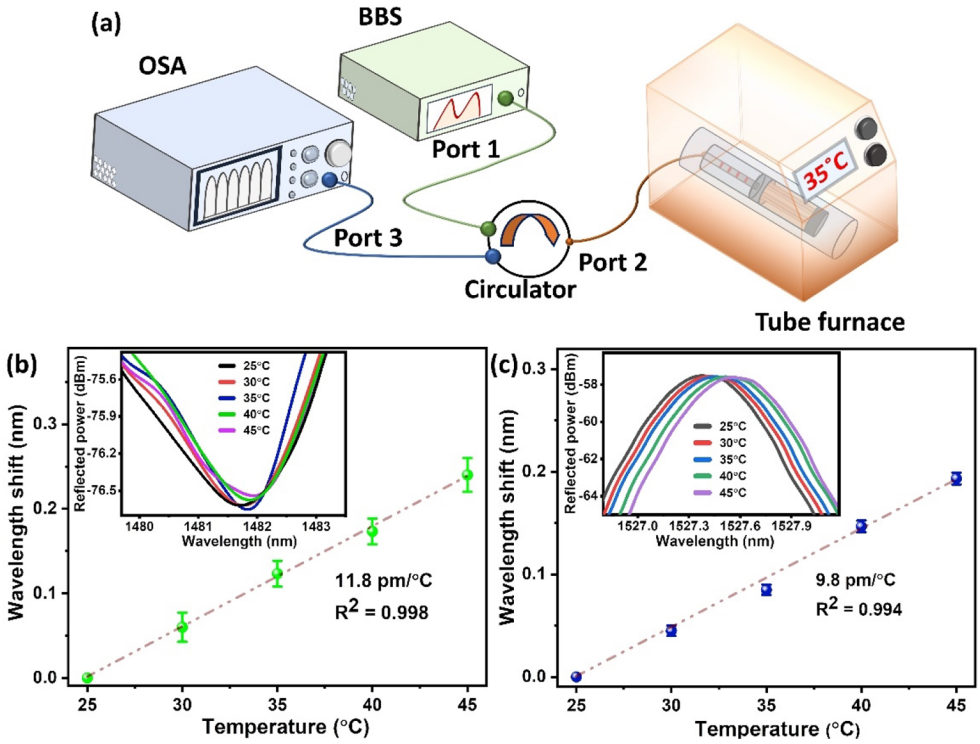

Fig. 9. Schematic of the temperature measurement (a), temperature response of the interference spectrum (b) and FBG (c).

5. Conclusion

A compact modal interferometer based optical fiber sensor coated with chitosan-PVA and GSH functionalized AuNPs has been demonstrated for lead ion detection. The fabrication of the interferometer has been accomplished by splicing a section of SMF with a small section of PCF. The tip of the PCF has been sealed by collapsing the air holes, thereby preventing the infiltration of liquids into the holes of PCF. Dip coating method has been followed to coat the PCF with chitosan-PVA and GSH functionalized AuNPs layers. Three probes have been fabricated following the similar approach and the maximum sensitivity response to the various concentrations of lead ions was found to be 0.031 nm/ppb along with a fast response time of ~10 s, while the dilution range of lead ions has been considered from 0 ppb to 50 ppb. Furthermore, the response of the sensor towards other heavy metal ions have been found to be insignificant. The temperature response of the probe has been studied by monitoring both the FBG peak and interference spectra, and the sensitivity has been found to be 9.8 pm/°C and 11.8 pm/°C, respectively. Therefore, the accurate response of the sensor towards lead analytes can be achieved by considering the temperature response of both these spectra. Thus, the proposed miniaturized sensor can easily be applied for eco-friendly detection of lead ions in water based medium.

Funding. Research Grants Council, University Grants Committee (15211317).

Disclosures. The authors declare no conflicts of interest.

Data availability. No data were generated or analyzed in the presented research.

Optics EXPRESS

References

1. K. Jomova and M. Morovič, "Effect of heavy metal treatment on molecular changes in root tips of Lupinus luteus L," Czech Journal of Food Sciences **27**, Effect of Heavy Metal Treatment on Molecular Changes in Root Tips of Lupinus luteus L. Czech J. Food Sci., 27: S386 (2009).
2. A. Tessier and D. R. Turner, *Metal speciation and bioavailability in aquatic systems* (Wiley Chichester, 1995).
3. P. K. Jha, S. K. Singh, S. Gatla, O. Mathon, S. Kurungot, and N. Ballav, "Pb2+- N Bonding Chemistry: Recycling of Polyaniline–Pb Nanocrystals Waste for Generating High-Performance Supercapacitor Electrodes," J. Phys. Chem. C **120**(2), 911–918 (2016).
4. S. Muralikrishna, D. Nagaraju, R. G. Balakrishna, W. Surareungchai, T. Ramakrishnappa, and A. B. Shivanandareddy, "Hydrogels of polyaniline with graphene oxide for highly sensitive electrochemical determination of lead ions," Anal. Chim. Acta **990**, 67–77 (2017).
5. C.-G. Elinder, L. Friberg, T. Kjellström, G. Nordberg, G. Oberdoerster, and W. H. Organization, "Biological monitoring of metals," (World Health Organization, 1994).
6. M. Ghaedi, F. Ahmadi, and A. Shokrollahi, "Simultaneous preconcentration and determination of copper, nickel, cobalt and lead ions content by flame atomic absorption spectrometry," J. Hazard. Mater. **142**(1-2), 272–278 (2007).
7. X. Chen, C. Han, H. Cheng, Y. Wang, J. Liu, Z. Xu, and L. Hu, "Rapid speciation analysis of mercury in seawater and marine fish by cation exchange chromatography hyphenated with inductively coupled plasma mass spectrometry," Journal of Chromatography A **1314**, 86–93 (2013).
8. E. K. Quagraine and V. P. Gadzekpo, "Studies of spectrophotometric reagents in some transition metal and lead ion-selective electrodes," Analyst **117**, 1899–1903 (1992).
9. A. Kumar, A. R. Chowdhuri, D. Laha, T. K. Mahto, P. Karmakar, and S. K. Sahu, "Green synthesis of carbon dots from Ocimum sanctum for effective fluorescent sensing of Pb2 + ions and live cell imaging," Sensors and Actuators B: Chemical **242**, 679–686 (2017).
10. Y. Wang, Z. Zhou, X. Qing, W. Zhong, Q. Liu, W. Wang, M. Li, K. Liu, and D. Wang, "Ion sensors based on novel fiber organic electrochemical transistors for lead ion detection," Anal. Bioanal. Chem. **408**(21), 5779–5787 (2016).
11. J.-H. Hwang, P. Pathak, X. Wang, K. L. Rodriguez, H. J. Cho, and W. H. Lee, "A novel bismuth-chitosan nanocomposite sensor for simultaneous detection of Pb (II), Cd (II) and Zn (II) in wastewater," Micromachines **10**(8), 511 (2019).
12. Z. Tou, T. Koh, and C. Chan, "Poly (vinyl alcohol) hydrogel based fiber interferometer sensor for heavy metal cations," Sensors Actuators B: Chemical **202**, 185–193 (2014).
13. Y.-N. Zhang, Y. Sun, L. Cai, Y. Gao, and Y. Cai, "Optical fiber sensors for measurement of heavy metal ion concentration: A review," Measurement **158**, 107742 (2020).
14. A. Al Noman, J. N. Dash, X. Cheng, C. Y. Leong, H.-Y. Tam, and C. Yu, "Hydrogel based Fabry-Pérot cavity for a pH sensor," Opt. Express **28**(26), 39640–39648 (2020).
15. M. Batumalay, M. A. M. Johari, M. I. M. A. Khudus, M. H. B. Jali, A. Al Noman, and S. W. Harun, "Microbottle resonator for temperature sensing," in *Journal of Physics: Conference Series*, (IOP Publishing, 2019), 012006.
16. J. N. Dash, X. Cheng, and H.-Y. Tam, "Low gas pressure sensor based on a polymer optical fiber grating," Opt. Lett. **46**(5), 933–936 (2021).
17. T. G. Giallorenzi, J. A. Bucaro, A. Dandridge, G. H. Sigel, J. H. Cole, S. C. Rashleigh, and R. G. Priest, "Optical fiber sensor technology," IEEE Trans. Microwave Theory Techn. **30**(4), 472–511 (1982).
18. M. A. M. Johari, A. Al Noman, M. A. Khudus, M. H. Jali, H. H. M. Yusof, S. W. Harun, and M. Yasin, "Microbottle resonator for formaldehyde liquid sensing," Optik **173**, 180–184 (2018).
19. C. Liu, Z. Sun, L. Zhang, J. Lv, X. Yu, and X. Chen, "Black phosphorus integrated tilted fiber grating for ultrasensitive heavy metal sensing," Sensors and Actuators B: Chemical **257**, 1093–1098 (2018).
20. B. S. Boruah and R. Biswas, "An optical fiber based surface plasmon resonance technique for sensing of lead ions: A toxic water pollutant," Opt. Fiber Technol. **46**, 152–156 (2018).
21. A. M. Shrivastav and B. D. Gupta, "Ion-imprinted nanoparticles for the concurrent estimation of Pb (II) and Cu (II) ions over a two channel surface plasmon resonance-based fiber optic platform," J. Biomed. Opt. **23**, 017001 (2018).
22. B. S. Boruah and R. Biswas, "In-situ sensing of hazardous heavy metal ions through an ecofriendly scheme," Optics & Laser Technology **137**, 106813 (2021).
23. B. H. Lee, Y. H. Kim, K. S. Park, J. B. Eom, M. J. Kim, B. S. Rho, and H. Y. Choi, "Interferometric fiber optic sensors," Sensors **12**(3), 2467–2486 (2012).
24. Y. Yin, S. Li, S. Wang, S. Jia, J. Ren, G. Farrell, E. Lewis, and P. Wang, "Ultra-high-resolution detection of Pb 2 + ions using a black phosphorus functionalized microfiber coil resonator," Photonics Res. **7**(6), 622–629 (2019).
25. S. H. K. Yap, Y.-H. Chien, R. Tan, A. R. bin Shaik Alauddin, W. B. Ji, S. C. Tjin, and K.-T. Yong, "An advanced hand-held microfiber-based sensor for ultrasensitive lead ion detection," ACS Sens. **3**(12), 2506–2512 (2018).
26. I. Yulianti, N. Putra, N. Akmalia, D. Pratiwi, and I. Albadiah, "Study of chitosan layer-based Fabry Perot Interferometer optical fiber sensor properties for detection of Pb2+, Hg2 + and Ni2+," in *J. Phys.: Conf. Ser.*, (IOP Publishing, 2019), 012079.
27. F. Chai, C. Wang, T. Wang, L. Li, and Z. Su, "Colorimetric detection of Pb2 + using glutathione functionalized gold nanoparticles," ACS Appl. Mater. Interfaces **2**(5), 1466–1470 (2010).

Optics EXPRESS

28. A. M. Shrivastav, D. S. Gunawardena, Z. Liu, and H.-Y. Tam, "Microstructured optical fiber based Fabry–Pérot interferometer as a humidity sensor utilizing chitosan polymeric matrix for breath monitoring," Sci. Rep. **10**(1), 6002 (2020).
29. J. N. Dash, R. Jha, and R. Das, "Micro-air cavity incorporated tapered-tip photonic crystal fiber based compact refractometer," Laser Phys. Lett. **17**(5), 055101 (2020).
30. C. Shao, H.-Y. Kim, J. Gong, B. Ding, D.-R. Lee, and S.-J. Park, "Fiber mats of poly (vinyl alcohol)/silica composite via electrospinning," Mater. Lett. **57**(9-10), 1579–1584 (2003).
31. A. Al Noman, J. N. Dash, X. Cheng, and C. Yu, "Fiber optic lead ion (Pb2+) sensor using chitosan diaphragm based Fabry-Pérot interferometer," in *Optoelectronics and Communications Conference*, (Optical Society of America, 2021), W3D. 2.
32. J. Du, J. Cipot-Wechsler, J. M. Lobez, H. P. Loock, and C. M. Crudden, "Periodic Mesoporous Organosilica Films: Key Components of Fiber-Optic-Based Heavy-Metal Sensors," Small **6**, 1168–1172 (2010).
33. A. D'Agostino, A. Taglietti, B. Bassi, A. Donà, and P. Pallavicini, "A naked eye aggregation assay for Pb 2 + detection based on glutathione-coated gold nanostars," J. Nanopart. Res. **16**, 1–11 (2014).